

1

2

Geophysical Research Letters

3

Supporting Information for

4

Relaxation of wind stress drives the abrupt onset of biological carbon uptake in the Kerguelen Bloom: a multisensor approach.

5

6

Violaine Pellichero¹, Jacqueline Boutin¹, Hervé Claustre², Liliane Merlivat¹, Jean-Baptiste Sallée¹, and Stéphane Blain³

7

8

¹Sorbonne Université, CNRS, IRD, MNHN, UMR 7159, Laboratoire d'Océanographie et du Climat : Expérimentations et Approches Numériques, LOCEAN-IPSL F-75005, Paris, France

10

11

² Sorbonne Université, CNRS, UMR 7093, Laboratoire d'Océanographie de Villefranche, LOV, 06230 Villefranche sur Mer, France

12

13

³Sorbonne Université, CNRS, UMR 7621, Laboratoire d'Océanographie MICrobienne, LOMIC, F-66650, Banyuls sur Mer, France

14

15

16

17

Contents of this file

18

19

Text S1 to S7

20

Figures S1 to S7

21

22

Introduction

23

In this Supplementary Information section, we introduce several figures as well as additional information in support of the main text. We give details on the methods used to estimate the mixed-layer depth based on the mooring data in one hand, and on the BGC-Argo floats in another hand. Moreover, we introduce the detailed decomposition of the net heat fluxes estimated from 4 different products and assess the wind contribution to the stratification of the water column. We also introduce additional information about the WMO 6902736 BGC-Argo float that are not shown in the main text. We fully describe the method to estimate the NCP based on DIC evolution. The dynamics of the phytoplankton bloom as observed on the BGC-Argo float data and on the mooring data is compared. This step allows us to be confident in considering the bloom development as a regional signal of the onset and not only as an advected patch of phytoplankton. Finally, we further investigate the vertical

24

25

26

27

28

29

30

31

32

33

34

35 structure of the surface layer to distinguish different dynamic within the mixing and
36 mixed-layer.

37 **Text S1. Testing the Mixed-layer Depth Calculation from Different Methods**

38 The ocean mixed-layer is commonly defined as the ocean surface layer in which
39 physical properties such as temperature, salinity, and density are well mixed, i.e., nearly
40 homogeneous with depth. The mixed-layer depth (MLD) has become a reference
41 concept in oceanography because it plays the essential role of intermediary between
42 the atmosphere and the deep ocean. A number of criteria have been developed over
43 the years to compute MLD based on a given density, salinity, or temperature profiles (de
44 Boyer Montégut et al., 2004; Holte & Talley, 2009).

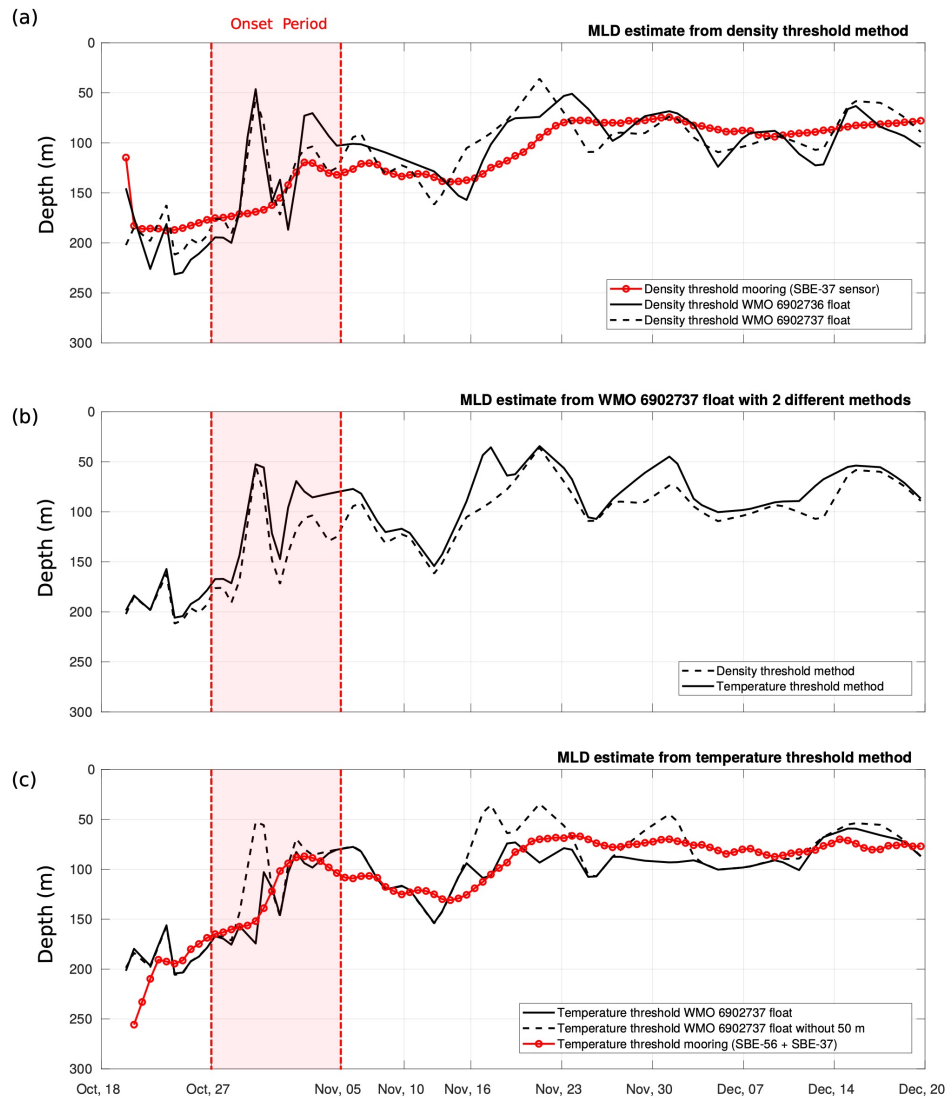
45 The most widespread method for finding the MLD is the threshold method which
46 search for the depth at which the temperature or density profiles change by a
47 predefined amount relative to the surface reference value. Moreover, it has been
48 shown that methods working on density profiles rather than temperature profiles are
49 more successful in detecting the base of the MLD (Sallée et al., 2006; Pellichero et al.,
50 2017). Based on such studies, we performed numerous tests in order to find the best
51 MLD estimate from our data. Our methods of MLD computation are all based on
52 individual profiles from BGC-Argo floats and mooring.

53 First, we compute the MLD with a density threshold criterion of $\Delta\sigma = 0.03 \text{ kg m}^{-3}$ as
54 shown in Figure. S1a. In black are plotted the two MLD from the two BGC-Argo floats
55 (WMO 6902737 in dashed black line and WMO 6902736 in black line), and in red is the
56 MLD estimated from the mooring which means this MLD is estimated only from the SBE-
57 37 sensors since they are the only ones that can provide salinity estimate and thus the
58 density. This result shows that the different MLD are consistent with each other and
59 there is a good correspondence between floats and mooring which gives us confidence
60 in our MLD estimate.

61 The calculation of the MLD is therefore equivalent according to the data (mooring
62 or BGC- Argo floats), but this is also true according to the detection methods used.
63 Indeed, in Figure. S1b we also compared the density threshold method (dashed black
64 line) with the temperature threshold method (black line) for WMO 6902737 float. Here
65 we use a temperature criterion for the detection of the base of the MLD about $\Delta T = 0.2$
66 $^{\circ}\text{C m}^{-1}$. Once again, the two methods are nearly the same. Following these tests, we
67 decided to work only with the temperature threshold method in order to use both SBE-
68 37 and SBE-56 mooring sensors and thus to improve the vertical resolution of the MLD
69 at the mooring.

70 Moreover, we remark in some points in Figure. S1a that the MLD estimate from the
71 BGC-Argo floats are shallower than those from the mooring. Therefore, we wondered if
72 the absence of data above 42 m may introduce errors in our estimation of the MLD from
73 the mooring. To tackle this question, we remove the data of the floats above 42 m and
74 we redo the same calculation of MLD. The result is introduced in Figure. S1c where we
75 can see the dashed black line which is the MLD estimate (from temperature threshold
76 method) from WMO 6902736 without any data above 42 m. Indeed, we notice that the
77 MLD without surface data is this time slightly deeper than the origin (black line) and is

78 getting closer to the MLD from the mooring (red line). This result suggests that
 79 sometimes the MLD from the mooring overestimates the MLD, but it occurs on rare
 80 occasions and practically not during the studied period of the onset of the
 81 phytoplankton bloom i.e. before November 05, 2016.



82

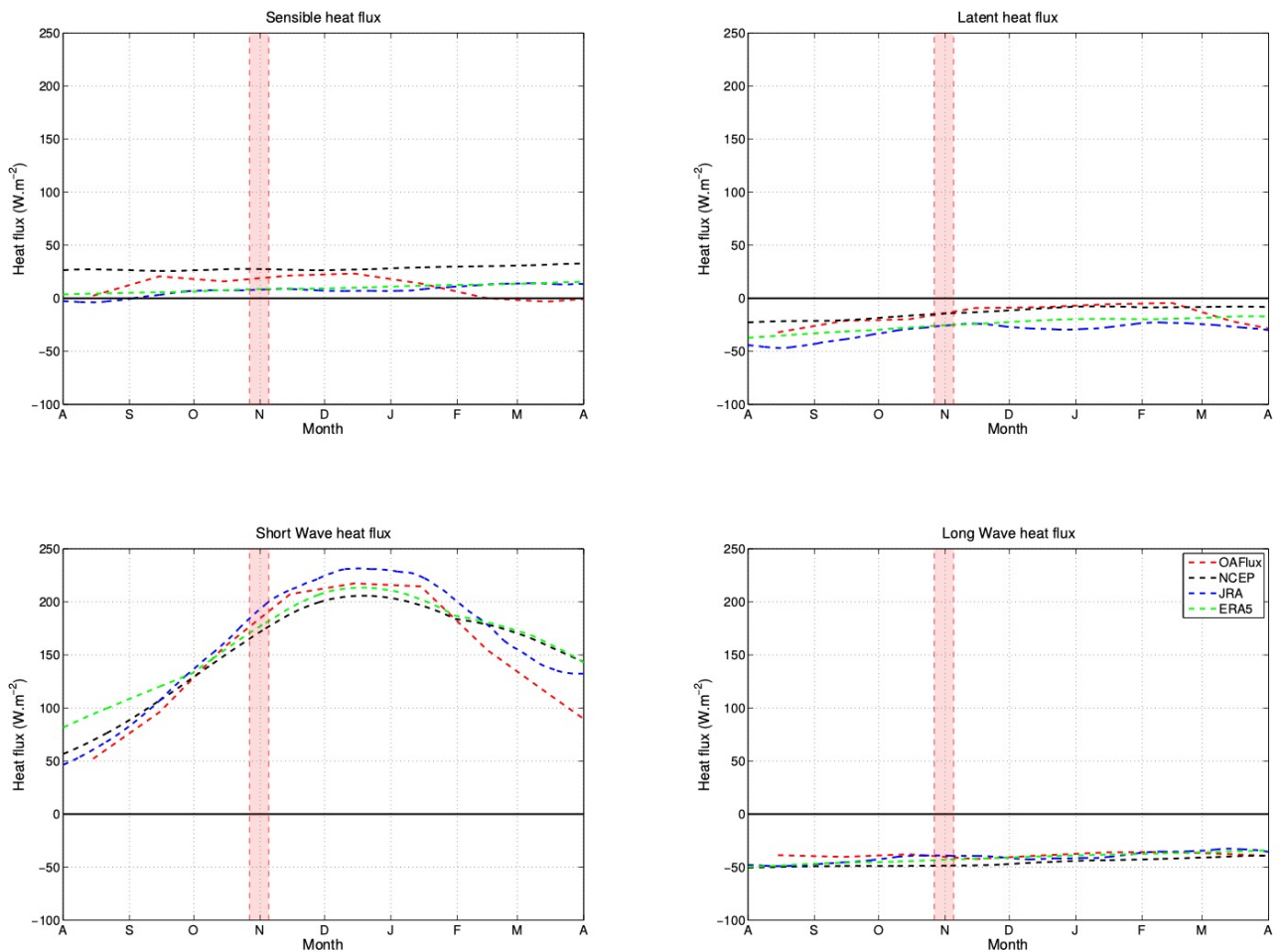
83 **Figure S1.** Mixed-layer depth estimates (in m) from different methods. (a) Time series of
 84 the MLD estimated from the density threshold method ($\Delta\sigma = 0.03 \text{ kg m}^{-3}$). The black lines
 85 are the MLD based on BGC-Argo floats and the red line is the MLD from the mooring
 86 (i.e. using only SBE-37 sensors that record the conductivity and allow to estimate the
 87 density). (b) Comparison between the MLD given by the density threshold method
 88 (dashed black line) and the temperature threshold method (black line, $\Delta T = 0.2 \text{ }^\circ\text{C m}^{-1}$)
 89 for the WMO 6902737 float. (c) Time series of the MLD presented in the main text and

90 estimated from the temperature threshold method based on the mooring (red line), the
91 WMO 6902737 float (black line) and the WMO 6902737 float where we previously
92 removed the data between 42 m up to the surface (dashed black line).

93

94 **Text S2. Relative Contributions to Heat Fluxes versus Wind**

95 The net heat flux shown in Figure. 2c is the sum of four contributions: latent flux (top
96 right panel), sensible flux (top left panel), short wave (bottom left) and longwave
97 (bottom right). All the 4 products used give consistent results and show that the net
98 heat flux was stabilizing the water column (positive values) since at least September
99 2016.



100 **Figure S2. Decomposition of the net heat flux into sensible heat flux (top right), latent**
101 **heat flux (top left), shortwave (bottom left) and longwave (bottom right). Each**
102 **component of the heat flux is shown for the 4 products used in this study from August**

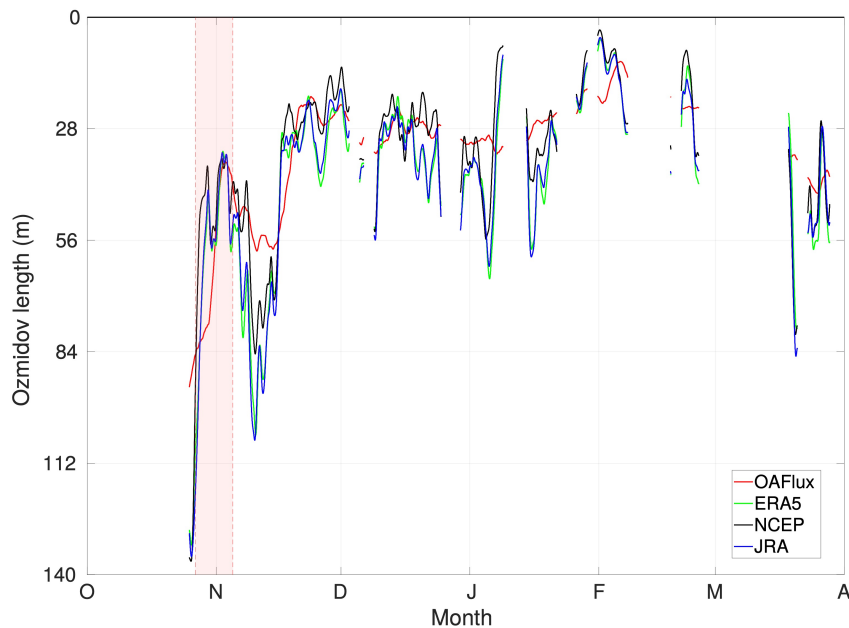
103 2016 to April 2017 (OAFflux in red, NCEP1 in black, JRA-55 in blue and ERA5 in green).
 104 The red shading indicates the onset period of the bloom (27 Oct to 5 Nov, 2016).

105

106 As the water column stratifies from at least September 2016, we investigated the wind
 107 stress (Figure. 2d) in order to explain how we can observe a rapid stratification of the
 108 MLD associated to the bloom at the end of October. Theoretical works indicates that
 109 when acting on a stratified fluid, the typical length scale where wind mixing acts, the
 110 “mixing-layer”, is the Ozmidov length (L_{OZ}) defined as (Denman and Gargett, 1983; Riley
 111 and Lelong, 2000; Brody and Lozier, 2015):

$$112 \quad L_{OZ} = (2\pi)\varepsilon^{1/2}N^{-3/2} \quad (A1)$$

113 Where N is the frequency of Brunt-Väisälä defined as $N^2 = -\frac{g}{\rho} \frac{\partial \rho}{\partial z}$ and ε is the rate of
 114 turbulent kinetic energy dissipation equal to $w_*^3/\kappa z$ at depth $z = 42 \text{ m}$, with w_* the
 115 friction velocity and κ the Von Kármán constant. The friction velocity at the mooring site
 116 is estimated from the wind-stress output of several different atmospheric reanalysis:
 117 $w_* = \sqrt{\tau/\rho}$, where τ is the wind-stress, and ρ is the sea-water density. At the mooring
 118 site we estimate N from its temperature contribution: $N^2 = -\alpha g \frac{\partial T}{\partial z}$, where α is the
 119 thermal contraction coefficient, and T is the water-column temperature estimated from
 120 the mooring temperature sensors. The gradient of temperature is estimated between
 121 42 m and the base of the mixed-layer.



122

123

124

125 **Figure S3. Mixing-layer estimated from the 4 products of wind stress used in this study**

126 (OAFflux in red, NCEP1 in black, JRA-55 in blue and ERA5 in green). The red shading

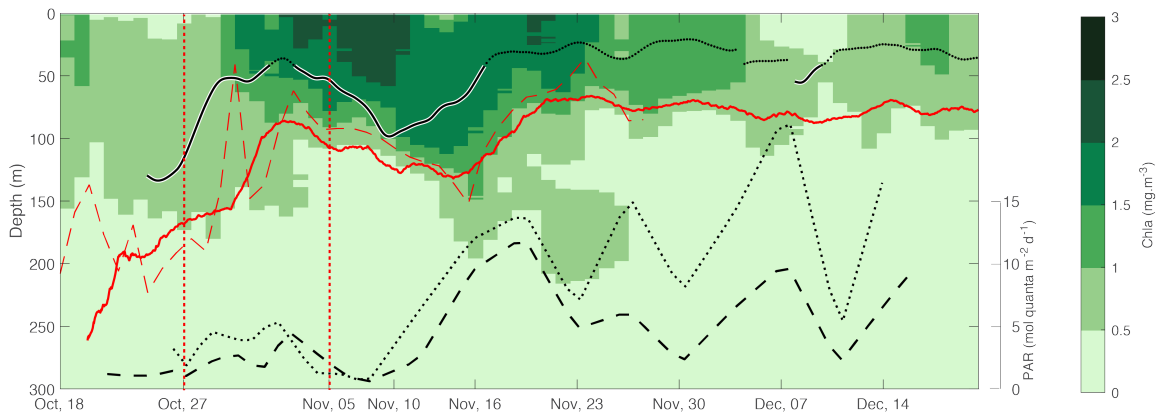
127 indicates the onset period of the bloom (Oct 27 to Nov 05, 2016)

128

129 The Figure. S3 showing the mixing-layer estimated from the 4 products, indicates that
 130 before the beginning of the bloom, the wind even if decreasing (Figure. 2d) was strong
 131 enough to mix the upper 130 m (according to NCEP1, ERA5 and JRA) and then balanced
 132 the stratifying effect of the heat flux. Then, right at the October 27, the mixing length
 133 reduces to 40-50 m as wind stress is still decreasing allowing the MLD to shoal, the
 134 vertical stratification to enhance and the bloom to initiate.

135 **Text S3. Data from the WMO 6902736 float**

136 Two BGC-Argo floats were deployed during the SOCLIM voyage. In this section we
 137 present the data from the WMO 6902736 BGC-Argo float. As mentioned in the main
 138 text, both results are very similar. As in Figure. 3d, we notice a large increase of the Chla
 139 during the onset period (27 Oct. to 05 Nov.).



140

141 **Figure. S4.** Vertical section of Chla (WMO 6902736 BGC-Argo float); MLD and mixing-
 142 layer computed at the mooring site are shown as plain red and black lines respectively,
 143 and MLD from the float time-series is shown as red dashed line for comparison; PAR_{MLD}
 144 and PAR_{MixLD} are shown as black dashed and dotted lines, respectively. The onset period
 145 of the bloom (October 27, 2016 to November 05, 2016) when DIC decreased linearly
 146 versus time (see Figure. 3b) is shown as the two vertical red dashed lines.

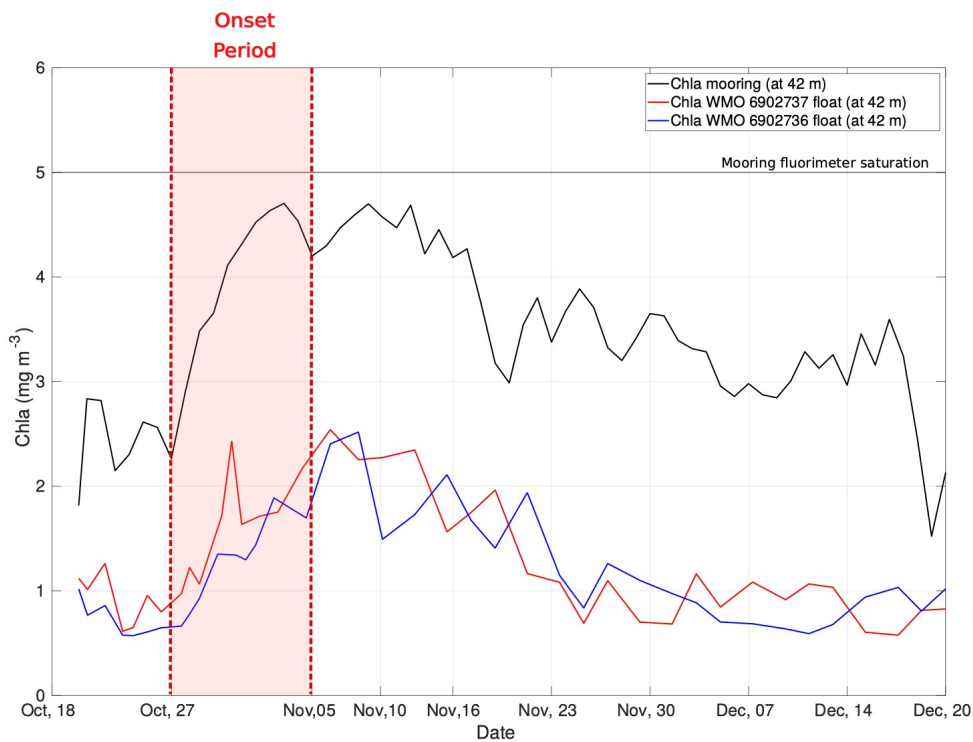
147

148 **Text S4. Eulerian VERSUS Lagrangian View: Comparison of the Dynamics of the Bloom**
 149 **from the Mooring and from the BGC-Argo Float**

150 The mooring is the Eulerian way to study the ocean as it is stationary at a fixed
 151 location. This has some implications for the results in terms of water mass advection for
 152 example. Indeed, when analyzing the onset of the phytoplankton bloom from mooring
 153 data, how to make sure that the mooring does not sample an advected water mass?
 154 One way to answer this question is to compare the dynamics of the phytoplankton
 155 bloom at the mooring point and the dynamics of the phytoplankton bloom seen by the
 156 BGC-Argo floats which provide Lagrangian measurements.

157 The Figure. S5 introduces such a comparison with the dynamics of the
 158 phytoplankton bloom seen by the mooring in black line and that record by the WMO
 159 6902737 float in red and WMO 6902736 in blue. In order to observe the same
 160 quantities, and knowing that the mooring fluorimeter is fixed at 42 m depth, we look at
 161 the Chla concentration at 42 m for the BGC-Argo floats. Two main differences remain
 162 between the mooring and the BGC-Argo floats: (1) the fluorimeter saturation level is at
 163 5 mg m^{-3} , which means that the Chla from the mooring may be higher, and (2) the
 164 values from the mooring are ~ 2.5 times higher than those record by the BGC-Argo floats
 165 partly due to different fluorimeters on the mooring and the BGC-Argo floats leading to
 166 difference of calibration (Roesler et al., 2017). Despite the differences limiting the
 167 analyse to relative variations rather than absolute values of Chla, the dynamics of the
 168 bloom development (the red area) recorded both from the mooring and the BGC-Argo
 169 floats is essentially identical with a sharp increase at the same period. This result
 170 indicates that what the mooring records in one location is not an advected patch of
 171 phytoplankton, but it is well representative of a regional signal of the onset of the
 172 bloom.

173
 174



175

176 **Figure S5.** Time series of the Chla concentration in mg m^{-3} . Comparison between the
 177 dynamics of the bloom recorded by the mooring at 42 m depth in black line and that
 178 recorded by the WMO 6902737 (red) and WMO 6902736 (blue) floats also at 42 m

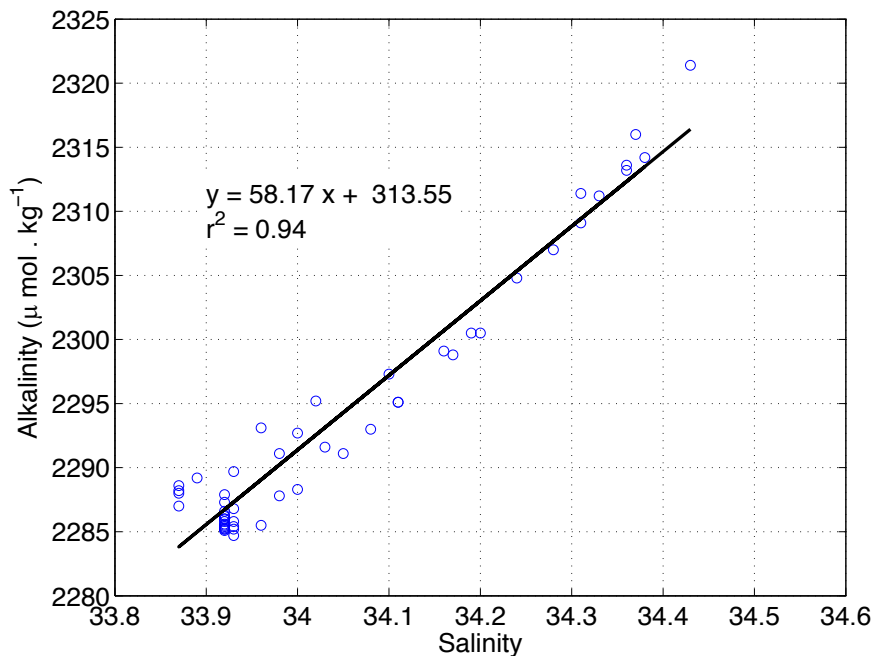
179 depth in red line. The horizontal line corresponds to the level of saturation of the
 180 mooring fluorimeter which is at 5 mg m⁻³.
 181

182 **Text S5. Quantitative Estimate of in-situ Net Community Production (NCP)**

183 **Calculation of DIC and Alkalinity:** Dissolved inorganic carbon, DIC (μmol kg⁻¹), is
 184 derived from pCO₂, alkalinity, temperature and salinity using the CO₂ dissociation
 185 constants of Mehrbach et al. (1973) as refitted by Dickson and Millero (1987). Alkalinity
 186 (Alk), is computed from salinity (Sal) using the alkalinity-salinity relationship (Figure. S6)
 187 derived from samples collected at a nearby location, station A3 (OISO cruise):

188
$$\text{Alk} = 58.17 \text{ Sal} + 313.55 \quad (r^2=0.94)$$

189 where Alk is expressed in μmol kg⁻¹. The relative precision of successive DIC values is
 190 expected to be 0.5 μmol kg⁻¹ (Merlivat et al, 2015).



191
 192 **Figure S6.** Relationship between alkalinity and salinity derived from the OISO cruises on
 193 October 2016 and January 2017 at the station A3. Solid line is linear fit through the data.

194

195 **Calculation of the air-sea CO₂ flux:** we estimated the air-sea CO₂ flux of 10.8
 196 mmol m⁻² d⁻¹ with the following equation:

197
$$\left(\frac{\Delta \text{DIC}}{\Delta t}\right)_{\text{air-sea}} = k \cdot s(p\text{CO}_{2\text{atm}} - p\text{CO}_{2\text{sea}}) \quad (\text{A2})$$

198 Where k is the gas transfer velocity (Wanninkhof, 2014), s is the solubility of CO_2 and
199 $p\text{CO}_{2\text{sea}}$ and $p\text{CO}_{2\text{atm}}$ are respectively the partial pressures of CO_2 in the water and in the
200 above lying air.

201

202 **Influence of eddy diffusion and of integration depth:** We perform sensitivity
203 test where we integrate NCP over the mixed-layer depth assuming a homogeneous
204 vertical DIC profile over the mixed-layer instead of over the mixing-layer depth and
205 where we additionally take into account a vertical eddy diffusion term as follows:

$$206 \quad NCP = \left(\frac{\Delta DIC_{int}}{\Delta t} \right)_{bio} = \left(\frac{\Delta DIC_{int}}{\Delta t} \right)_{meas} - k \times s \times (p\text{CO}_{2atm} - p\text{CO}_{2sw}) - K_z \times \frac{dDIC}{dz} \quad (\text{A2})$$

207 The eddy diffusion term, is estimated to be $7.8 \text{ mmol m}^{-2} \text{ d}^{-1}$ (i.e. less than 4 % of
208 the NCP) using a spatially constant vertical diffusion coefficient of $K_z = 3.10^{-4} \text{ m}^2 \text{ s}^{-1}$ (Park
209 et al., 2008) and the vertical gradient of DIC recorded at the basis of the mixed-layer
210 during the OISO cruise on the 18th and 24th October, 2016 ($dDIC/dz = 0.3 \text{ } \mu\text{mol kg}^{-1} \text{ m}^{-1}$).
211 Hence it is negligible in front of the NCP integrated in the mixed-layer ($212 \text{ mmol m}^{-2} \text{ d}^{-1}$).
212 Since we expect the DIC gradient at the basis of the mixing-layer to be less than the
213 one at the basis of the mixed-layer, the influence of the eddy diffusion term on the
214 estimate of NCP integrated over the mixing-layer is expected to be less than 7.8 mmol.
215 $\text{m}^{-2} \text{ d}^{-1}$, i.e. an uncertainty less than 7%.

216

217 **Text S6: Chla climatology computation**

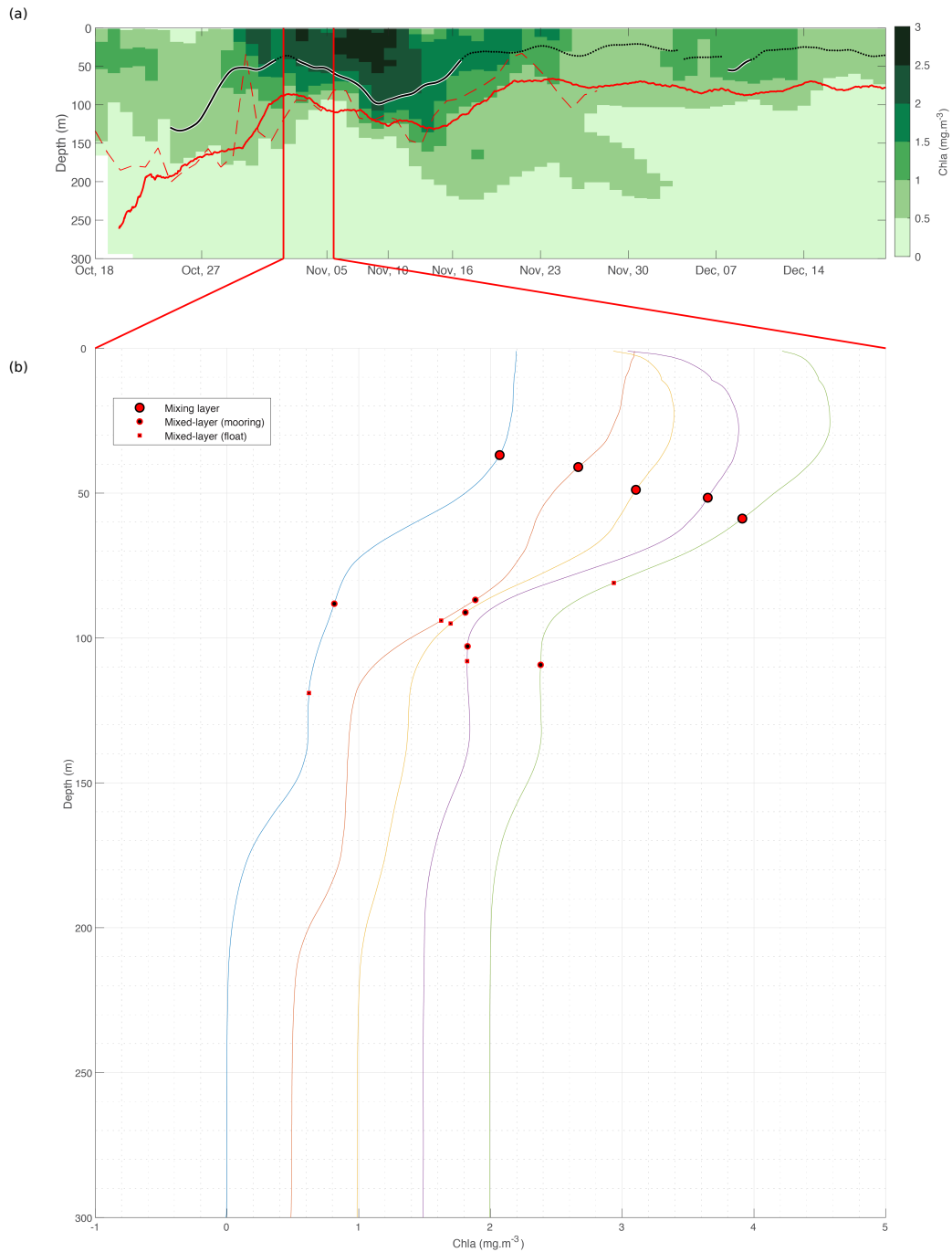
218 We used a climatology of satellite Chla data processed and distributed by ACRI-ST
219 GlobColour service (<http://marine.copernicus.eu>) to describe the seasonal cycle of Chla
220 averaged at the mooring site. The climatology (1998-2017) is created using data falling
221 into a moving temporal window of ± 5 days (i.e. 11 days).

222

223 **Text S7: Chla in MLD and mixing-layer**

224

225 In this section, we look at specific Chla profiles to convince ourself that there is indeed a
226 different dynamic within the mixing and mixed-layer. It is clear both on the vertical
227 section (upper panel, Figure. S7) and even more obviously on a set of individual profiles
228 (lower panel, Figure. S7), that there is a two-layer structure within the MLD. While the
229 upper 50 meters or so are associated with high Chla concentration, the lower part of the
230 MLD have much weaker Chla concentration. This structure within the MLD is very
231 suggestive that the MLD is not actively mixed during this time. Now, plotting the
232 estimated mixing-layer depth, it shows clearly that the high Chla concentration in the
233 upper part of the MLD is within the mixing-layer (Figure. S7b). The estimated mixing-
234 layer depth predicts impressively well the vertical boundary, within the MLD, separating
235 high Chla concentration in the upper part of the MLD, with sharp decrease with depth of
236 Chla concentration in the lower part of the MLD.



237
 238
 239
 240
 241

Figure S7. (a) Same as Figure. 3d (WMO 6902737 BGC-Argo float). (b) A set of individual Chla profiles with mixed-layer depths estimates from the mooring (black circle), from the BGC-Argo float (black square) and mixing-layer depths (red circle).